Letter

Importance of vibrational anharmonicity for electron-phonon coupling in molecular crystals

Antonios M. Alvertis [1,2,*] and Edgar A. Engel[1,†]

[1]*Cavendish Laboratory, University of Cambridge, J. J. Thomson Avenue, Cambridge CB3 0HE, United Kingdom*
[2]*Materials Sciences Division, Lawrence Berkeley National Laboratory, Berkeley, California 94720, USA*

(Received 18 January 2022; revised 4 April 2022; accepted 20 April 2022; published 6 May 2022; corrected 25 July 2022)

Accurate predictions of electronic band gaps are key to the computational design of functional materials with tailored optical and thermoelectric properties. While an accurate description of the underlying electronic structure is indispensable, electron-phonon interactions also play a prominent role in determining the band gap. The harmonic vibrational approximation is used almost universally to describe electron-phonon coupling and provides a satisfactory description in most systems. Here, we demonstrate that this is not the case for molecular crystals due to the presence of strongly anharmonic motions. We demonstrate the breakdown of the harmonic approximation in acene molecular crystals, and show that converged band gaps can be obtained by rigorously accounting for vibrational anharmonicity using path-integral molecular dynamics. Finally, we characterize the most anharmonic vibrational modes and their contributions to the band-gap renormalization.

DOI: 10.1103/PhysRevB.105.L180301

Introduction. Electronic band gaps are a key quantity in studying the optical and electrical properties of materials and are central to applications such as photovoltaics [1] and thermoelectrics [2]. Accurate predictions of band gaps are critical in understanding how the electronic and optical properties may be tuned by factors such as atomic or molecular substitutions, temperature [3–5], and pressure [6,7], and thus for the design of materials with tailored characteristics. General predictive calculations of the electronic properties of materials require not only an accurate description of the electronic structure of a fixed atomic configuration, but also the rigorous treatment of quantum and thermal nuclear fluctuations, which can lead to a significant renormalization and temperature dependence of band gaps [8,9].

Traditionally this electron-phonon coupling is either neglected, or accounted for subject to approximations [4]. In particular, nuclear motion is generally assumed to be harmonic, in which case the nuclear density distribution can be computed analytically and used to sample the ensemble-average band gap [4]. This approach has proven practical and suitable for a wide range of semiconductors [8–10]. Unfortunately, the harmonic vibrational approximation (HA) breaks down for general molecular systems. This is well established in the context of computing thermodynamic stability [11–16], but more rarely discussed in the context of electron-phonon coupling and computational spectroscopy.

In this Letter, we calculate fully anharmonic, quantum-mechanical, finite-temperature electronic band gaps, and identify the phonons that most strongly deviate from the harmonic behavior. This is achieved by employing path-integral molecular dynamics (PIMD) to sample the full anharmonic, quantum-mechanical thermodynamic ensemble and subsequently computing the associated band gaps. To render these otherwise prohibitively expensive PIMD simulations feasible, we use a surrogate machine-learning (ML) potential, constructed to reproduce the potential energy surface from first-principles density functional theory (DFT) calculations. We restrict ourselves to DFT electronic band gaps, reserving the extension to more sophisticated techniques for future work. While DFT using (semi)local density functionals tends to severely underestimate band gaps [17,18], it provides the foundation for more accurate but computationally demanding techniques such as diffusion Monte Carlo [19] and *GW* many-body perturbation theory [20].

Using the example of the acene molecular crystals, we highlight the catastrophic failure of band-gap calculations based on the HA in the presence of anharmonic crystal vibrations, and identify which phonons dominate the electron-phonon interaction at different temperatures. Our approach could be utilized to rigorously compute the band gaps of various materials where anharmonicity becomes important, such as lead-halide perovskites [21,22].

Systems and methods. To demonstrate the impact of nuclear vibrational anharmonicity on electron-phonon coupling in organic molecular crystals, we use the acene series, including naphthalene (Np), anthracene (Ac), tetracene (Tc), and pentacene (Pc). These systems consist of an increasing number of fused benzene rings (see Fig. 1, top left panel). In every case we report the minimum band gap of the studied systems. The electronic and optical properties of these acenes have been the topic of a previous study, which found evidence of strong effects of anharmonicity [23]. Details regarding the structures, geometry optimizations, etc., are provided in Supplemental Material [24] Sec. II A.

We compute first-principles ensemble-average band gaps within the adiabatic approximation

$$E_g = \langle E_g(X) \rangle_{\mathcal{H}} = \frac{1}{Z} \int dX E_g(X) e^{-\beta V(X)}, \qquad (1)$$

*amalvertis@lbl.gov
†eae32@cam.ac.uk

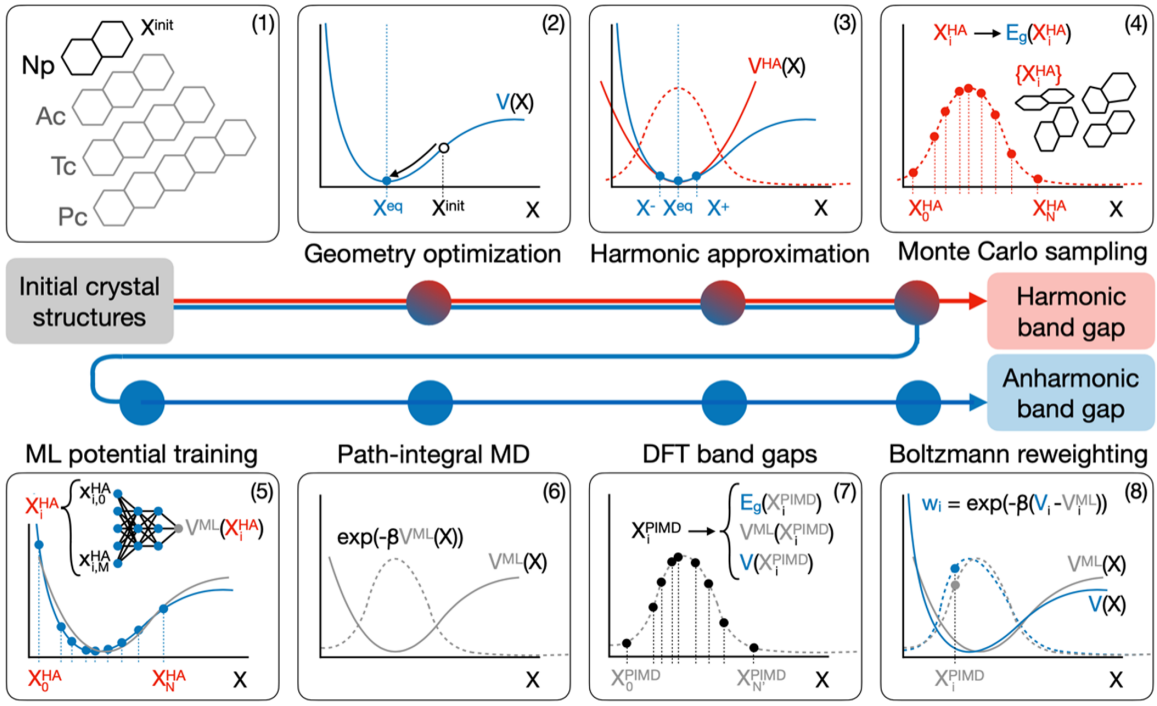

FIG. 1. Schematic of the key steps in obtaining first-principles band gaps within the harmonic approximation, and upon rigorous sampling of anharmonic quantum nuclear fluctuations. For simplicity, we show a single (phonon) degree of freedom X. The approximate harmonic potential $V^{\mathrm{HA}}(X)$ (solid line), the corresponding Gaussian probability distribution (dashed line), and samples X^{HA} drawn therefrom (solid circles) are highlighted in red, while the approximate surrogate ML potential $V^{\mathrm{ML}}(X)$ and associated probability distribution and samples are shown in gray, and the rigorous, first-principles potential $V(X)$, distribution, and Boltzmann weights are indicated in blue. The crystal structures are represented in terms of their molecular building blocks.

where the canonical partition function $Z = \int dX e^{-\beta V(X)}$ involves the configuration space integral $\int dX$ [25]. We pursue a three-pronged approach. We first geometry optimize the different acenes (Fig. 1, panel 2), and extract the respective "static" band gaps E_g^{st}, which provide the reference for computing vibrational band-gap corrections.

Second, we compute the band gap within the HA, which amounts to approximating the physical Hamiltonian $\mathcal{H}$ with

$$\mathcal{H}^{\mathrm{HA}} \equiv \frac{1}{2}\sum_{n,\mathbf{q}} \nabla^2_{u_{n,\mathbf{q}}} + V^{\mathrm{HA}}, \quad V^{\mathrm{HA}} \equiv \frac{1}{2}\sum_{n,\mathbf{q}} \omega^2_{n,\mathbf{q}} u^2_{n,\mathbf{q}} \qquad (2)$$

(in atomic units). This primarily serves the purpose of providing atomistic insight by resolving the phonons, labeled by branch index n and wave vector $\mathbf{q}$, and (subsequently) their respective contributions to the vibrational band-gap correction. We compute the ensemble-average E_g^{HA} using a finite-displacement approach [26,27] to compute phonon frequencies $\{\omega_{n,\mathbf{q}}\}$ and coordinates $\{u_{n,\mathbf{q}}\}$ (Fig. 1, panel 3), and then draw N random samples $\{X_i^{\mathrm{HA}}\}$ from the multivariate Gaussian phonon distribution and calculate their band gaps $\{E_g(X_i^{\mathrm{HA}})\}$ (Fig. 1, panel 4). E_g^{HA} is then simply computed as the average band gap of the samples

$$E_g^{\mathrm{HA}} = \lim_{N\to\infty} \frac{1}{N}\sum_{i=1}^{N} E_g\left(X_i^{\mathrm{HA}}\right). \qquad (3)$$

This provides a nonperturbative description of electron-phonon coupling [8], *within the constraints of the approximate harmonic vibrational distribution*. Unfortunately, the systematic error resulting from the HA cannot be quantified reliably.

To rigorously account for general, anharmonic quantum nuclear motion we finally employ path-integral techniques. Since converged first-principles PIMD simulations for our structures are prohibitively expensive, we use the total energies and forces computed as a side product of sampling E_g^{HA} to train a surrogate ML potential V^{ML} (gray solid, Fig. 1, panel 5). We chose the tried-and-tested Behler-Parinello framework as implemented in the N2P2 package [28], in which structures are encoded in atom-centered symmetry functions [29] and passed through fully connected feedforward artificial neural networks to compute atomic forces and contributions to the total energy. We replicate the architecture, which has previously proven highly accurate and reliable for polymorphs of benzene [30,31]. In result, the evaluation of V^{ML} is orders of magnitude less expensive than a corresponding first-principles calculation, which renders PIMD simulations using the ML Hamiltonian,

$$\mathcal{H}^{\mathrm{ML}} \equiv \sum_{i=1}^{N_a} \frac{\hat{\mathbf{p}}_i^2}{2m_i} + V^{\mathrm{ML}}(\hat{\mathbf{r}}_1, \ldots, \hat{\mathbf{r}}_{N_a}), \qquad (4)$$

computationally tractable. This permits us to compute the band gap of the ML ensemble as the average over the DFT values computed for a small number N' of sample structures

$\{X_i^{\mathrm{ML}}\}$ drawn from a PIMD trajectory:

$$E_g^{\mathrm{ML}} = \lim_{N'\to\infty} \frac{1}{N'} \sum_{i=1}^{N'} E_g\left(X_i^{\mathrm{ML}}\right). \tag{5}$$

In practice we find that computing the DFT band gap for between 50 (for the larger supercells) and 200 (for the unit cells) configurations from PIMD trajectories for 32 beads at regular intervals of 50 fs, provides suitably converged ensemble-average band gaps.

Crucially, the affordability of V^{ML} comes at the price of residual errors with respect to the reference V, which may arise from the short-ranged nature of the ML potential [32], information lost during the "featurization" of the samples [33], or from limited data. While the root-mean-squared (rms) errors in ML energies and forces do not exceed 3.1 meV/atom and 0.16 eV/Å, except for naphthalene, they stand to affect the band-gap estimates. To quantify this we use the first-principles potentials $\{V(X_i^{\mathrm{ML}})\}$, which come as a complement of evaluating the corresponding band gaps [Eq. (5)], to extract the first-principles band gap E_g by statistical reweighting of the samples obtained from the ML ensemble (Fig. 1, panel 8):

$$E_g = \lim_{N'\to\infty} \frac{\sum_{i=1}^{N'} w\left(X_i^{\mathrm{ML}}\right) E_g\left(X_i^{\mathrm{ML}}\right)}{\sum_{i=1}^{N'} w\left(X_i^{\mathrm{ML}}\right)},$$

$$w_i \equiv \exp\left\{-\beta\left[V\left(X_i^{\mathrm{ML}}\right) - V^{\mathrm{ML}}\left(X_i^{\mathrm{ML}}\right)\right]\right\}. \tag{6}$$

Recovering the DFT band gaps E_g for the unit cells of acenes using Eq. (6) reveals a consistent overestimation of the band-gap correction for all acenes using V^{ML}, which does not affect the trends and microscopic insights discussed below. This overestimation is largest for naphthalene (97 meV) and much smaller for the larger acenes, consistent with smaller errors in V^{ML} for these systems.

For the acenes, applying the same reweighting strategy to recover E_g from the sampled $\{E_g(X_i^{\mathrm{HA}})\}$ is prevented by substantial differences between $V^{\mathrm{HA}}(X)$ and $V(X)$, leading to diverging weights and unphysical band-gap estimates, which do not agree with those obtained using PIMD. However, since statistical reweighting can be attempted at no additional cost in terms of DFT calculations, for near-harmonic systems it provides a practical means of probing for anharmonic effects and avoiding unnecessary PI calculations.

Results. Let us demonstrate the breakdown of the HA in the case of anthracene at $T = 300$ K. As visualized in Fig. 2(a), the harmonic correction to the static band gap (red) fails to converge with increasing supercell size. Meanwhile, accounting for anharmonic effects leads to smooth convergence up to large, size 27 ($3 \times 3 \times 3$) supercells. To elucidate the disagreement between the two cases, we project the harmonic and anharmonic trajectories of anthracene onto the phonon coordinates $\{u_{n,\mathbf{q}}\}$. This allows us to compare the rms displacement $\sqrt{\langle u_{n,\mathbf{q}}^2 \rangle}$ of each phonon mode $(n, \mathbf{q})$ at the two levels of theory. Figure 2(b) shows significant differences in the rms displacements of low-frequency phonons, and highlights two particularly anharmonic modes (black circle and arrow) that involve sliding motions between several anthracene molecules as shown in the inset. In Fig. 2(c) we

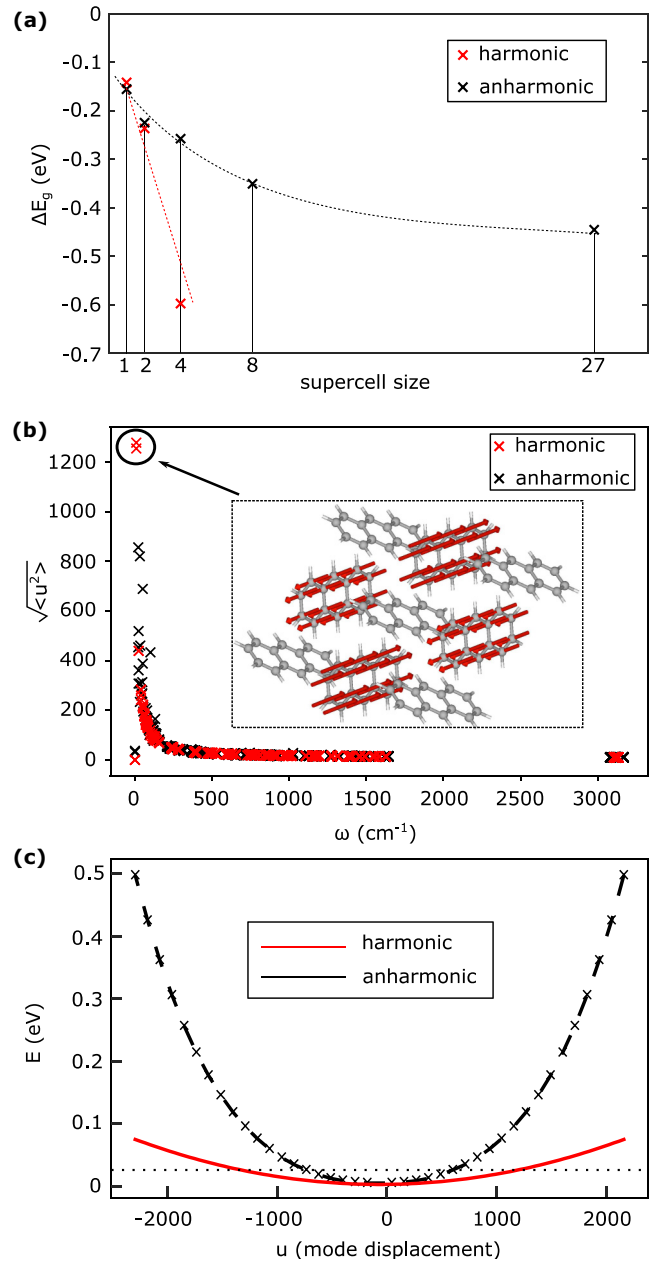

FIG. 2. Harmonic and anharmonic renormalisation of the anthracene bandgap at 300 K (panel a). The root-mean-squared phonon displacements of the two distributions (panel b) highlight unphysical displacements for harmonic low-frequency phonons, in particular for those involving a sliding motion between several molecules (inset). Panel c shows the corresponding harmonic and anharmonic potential energy surface, where room temperature is marked with a dotted line.

plot the harmonic potential energy surface along the phonon coordinate $u_{n,\mathbf{q}}$ of one of the two modes and compare it to the true, fully anharmonic potential along $u_{n,\mathbf{q}}$ as obtained through direct DFT calculations. We see that the true potential is much stiffer than its HA and, in comparison, stifles the amplitude of the vibrational motion. This is consistent with the corresponding harmonic and anharmonic rms displacements observed in Fig. 2(b), and suggests that the HA leads

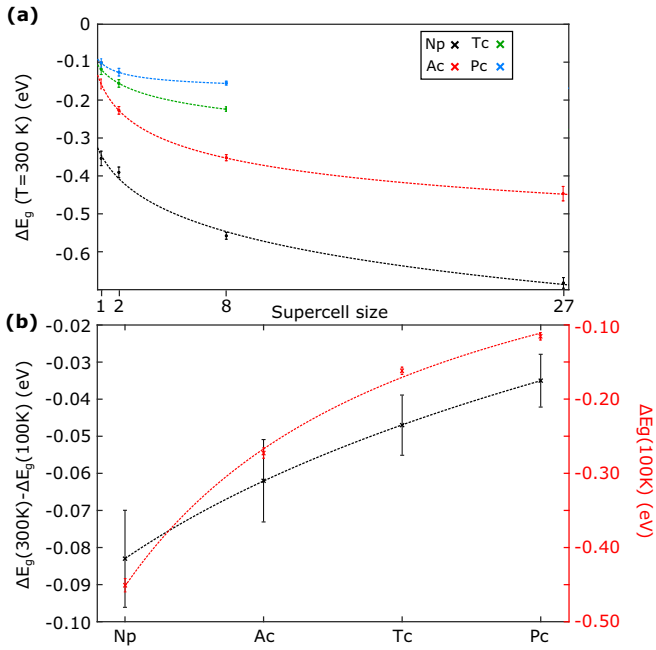

FIG. 3. Band-gap renormalization of the acene crystals, computed with path-integral molecular dynamics. (a) Convergence of the band-gap correction at 300 K with respect to the simulation cell size. (b) shows the difference between the converged 100- and 300-K corrections (black), as well as the band-gap renormalization at 100 K (red).

to unphysically large phonon amplitudes, which in turn result in the lack of convergence for the harmonic band gap seen in Fig. 2(a).

The breakdown of the HA is not limited to the case of anthracene. In Supplemental Material [24] Sec. III, we show that the remaining acenes exhibit similar behavior, with strongly anharmonic low-frequency phonons, which can in turn manifest a similar lack of convergence for the harmonic band gap. Such anharmonicity generally arises when studying supercells of size four or above, where phonons can primarily involve intermolecular motion between several molecules, resulting in extremely low-frequency anharmonic motion, particularly for (but not limited to) acoustic modes. Consequently, studies using coarse $\mathbf{q}$ grids (or, conversely, small simulation cells within finite-displacement approaches) may escape the breakdown of the HA and obtain reasonable estimates of vibrationally renormalized band gaps of molecular crystals [23]. However, this generally comes at the price of errors due to unconverged $\mathbf{q}$ sampling (in particular, neglecting low-frequency $\mathbf{q} \rightarrow \mathbf{0}$ phonons), as apparent in Figs. 2(a) and 3(a). Accurate band-gap predictions thus require studying large supercells, which exhibit strong anharmonicity. Notably, the degree of anharmonicity is fairly insensitive to the flavor of electronic structure theory, as shown for pentacene in Supplemental Material [24] Sec. III.

Therefore, in order to rigorously account for electron-phonon interactions in molecular crystals, we turn to the aforementioned PIMD approach, which fully accounts for anharmonicity and nuclear quantum effects. Figure 3(a) shows that the room-temperature band-gap renormalization of the acene crystals converges smoothly with increasing supercell size. Pentacene and tetracene band gaps are already reasonably well converged for supercells of size two. The band gaps only show marginal changes when increasing the supercell size to eight, which is the maximum we were able to simulate for these systems, due to memory limitations in the DFT band-gap calculations for the sampled configurations. For the smaller acenes, larger supercells are required to reach convergence and even for the $3 \times 3 \times 3$ case naphthalene and anthracene seem to not be fully converged. However, DFT calculations on larger supercells are prohibitively expensive. More details regarding the convergence of PIMD averages are given in Supplemental Material [24] Sec. II.

Comparing our value of -0.683 eV for the room-temperature band-gap renormalization in naphthalene to the -0.44 eV [34] obtained using density functional perturbation theory (DFPT) [35,36] and Allen-Heine-Cardona (AHC) theory highlights the differences arising from different approximations to the electron-phonon interaction. While Ref. [34] relies on the HA and perturbation theory, our PIMD approach naturally includes anharmonicity and higher-order terms in the electron-phonon interaction. The latter are known to be important in molecular crystals [8] and are reflected, for instance, in the nonquadratic dependence of the pentacene band gap on the displacement of low-frequency phonons shown in Supplemental Material [24] Fig. 4(b). We also note that the lack of convergence of the band gap that we observe within the HA is not related to the divergence which can appear in AHC theory, particularly for IR-active materials [37], where it can be remedied by including nonadiabatic effects. We expect our results for the acene crystals (unlike more ionic materials [38]) to be insensitive to nonadiabatic effects. Moreover, we emphasize that the unphysical effects that arise from neglecting the effects of anharmonicity on electron-phonon coupling are not an artifact of finite displacement methods, as similar observations have been reported for $SrTiO_3$ within AHC theory [39].

Figure 3(a) highlights larger band-gap corrections for smaller molecular crystals. It is however not yet clear whether the differences in the band-gap renormalization of the acenes are due to thermal or quantum nuclear motion. To answer this question, we also sample the band gaps at 100 K using PIMD. In Fig. 3(b), we plot the difference between the band gaps at 100 and 300 K (black). This purely temperature-driven renormalization is more pronounced for smaller acenes, indicating that thermally activated low-frequency phonons are more strongly coupled to the band gaps of these systems. The remaining band-gap renormalization at 100 K (red) is also stronger for the smaller systems. At low temperatures nuclear quantum fluctuations due to high-frequency phonons dominate, since thermal activation is minimal, while these modes have significant zero-point energies $\hbar\omega_{n,\mathbf{q}}/2$. To further elucidate the different couplings of low- and high-frequency phonons to the acene band gaps, we compute the phonon-resolved band-gap renormalization within a quadratic approximation, which confirms the above picture (see Supplemental Material [24] Sec. IV).

Finally, it is interesting to visualize the phonons which most strongly couple to electrons as a result of thermal activation (see Supplemental Material [24] Sec. V). Rotations

around the molecular long axes lead to significant band-gap renormalization in all studied systems, and increasingly so for the smaller acenes. Naphthalene is the only system with significant contributions from rotations around the molecular short axis, which drive the failure of the harmonic approximation. We hypothesize that such short-axis rotations become energetically unfavorable for larger acenes, increasing the frequency of these phonons beyond the threshold of thermal activation at room temperature. Highly anharmonic sliding motions [such as the one in Fig. 2(b)] become important in the larger acenes and result in a *blueshift* of the gap (see Supplemental Material [24] Sec. III). The anharmonic character of these motions, as well as their importance for phenomena such as charge transport and singlet fission in organic crystals, are well known [40–42].

Conclusions. In this Letter we have demonstrated the breakdown of the HA for computing electron-phonon effects and associated thermodynamic averages of observables for molecular crystals. We have presented an integrated approach for rigorously including anharmonic effects in calculations of electron-phonon coupling within the adiabatic approximation, showing that it permits computing converged values for the phonon-induced band-gap renormalization of the acene crystals. We find that both low- and high-frequency vibrations couple more strongly to the band gap of crystals consisting of smaller molecules, which we discuss in light of the displacement patterns of specific phonon modes. Sliding motions are consistently found to be among the most anharmonic ones, emphasizing the need to rigorously include anharmonicity in the study of phenomena such as charge transport and singlet fission where these are known to be important.

In the acenes the breakdown of the HA is driven by low-frequency acoustic phonons, which are only probed for fine sampling of the Brillouin zone. However, vibrational anharmonicity is a recurrent theme in functional materials and more generally plays prominent roles in determining material properties, such as in the dynamic stabilization of halide perovskites [43] and the cubic perovskite phase of $SrTiO_3$ [14]. We thus emphasize that our approach for capturing anharmonic effects is universal (albeit subject to the adiabatic approximation) and applicable to diverse materials. Given the demonstrable importance of nonadiabatic effects for electron-phonon coupling in more ionic materials [38], it will be interesting to investigate the interplay of nonadiabaticity and vibrational anharmonicity.

Acknowledgments. The authors thank Bartomeu Monserrat (Cambridge), Jonah B. Haber (Berkeley), and Jeffrey B. Neaton (Berkeley) for insightful discussions. A.M.A. acknowledges funding from the Winton Programme for the Physics of Sustainability. E.A.E. acknowledges funding from Trinity College, Cambridge, through a Junior Research Fellowship. Part of the calculations were performed using resources provided by the Cambridge Tier-2 system operated by the University of Cambridge Research Computing Service [44] and funded by EPSRC Tier-2 capital Grant No. EP/P020259/1.

[1] M. A. Green, Photovoltaic technology and visions for the future, Prog. Energy **1**, 013001 (2019).
[2] J. O. Sofo and G. D. Mahan, Optimum band gap of a thermoelectric material, Phys. Rev. B **49**, 4565 (1994).
[3] P. B. Allen and V. Heine, Theory of the temperature dependence of electronic band structures, J. Phys. C **9**, 2305 (1976).
[4] S. Poncé, G. Antonius, Y. Gillet, P. Boulanger, J. Laflamme Janssen, A. Marini, M. Côté, and X. Gonze, Temperature dependence of electronic eigenenergies in the adiabatic harmonic approximation, Phys. Rev. B **90**, 214304 (2014).
[5] W. A. Saidi, S. Poncé, and B. Monserrat, Temperature dependence of the energy levels of methylammonium lead iodide perovskite from first-principles, J. Phys. Chem. Lett. **7**, 5247 (2016).
[6] S. K. Yadav, T. Sadowski, and R. Ramprasad, Density functional theory study of ZnX (X = O, S, Se, Te) under uniaxial strain, Phys. Rev. B **81**, 144120 (2010).
[7] V. Gorelov, M. Holzmann, D. M. Ceperley, and C. Pierleoni, Energy Gap Closure of Crystalline Molecular Hydrogen with Pressure, Phys. Rev. Lett. **124**, 116401 (2020).
[8] B. Monserrat, E. A. Engel, and R. J. Needs, Giant electron-phonon interactions in molecular crystals and the importance of nonquadratic coupling, Phys. Rev. B **92**, 140302(R) (2015).
[9] G. Antonius, S. Poncé, P. Boulanger, M. Côté, and X. Gonze, Many-Body Effects on the Zero-Point Renormalization of the Band Structure, Phys. Rev. Lett. **112**, 215501 (2014).
[10] P. Han and G. Bester, Large nuclear zero-point motion effect in semiconductor nanoclusters, Phys. Rev. B **88**, 165311 (2013).
[11] O. Hellman, I. A. Abrikosov, and S. I. Simak, Lattice dynamics of anharmonic solids from first principles, Phys. Rev. B **84**, 180301(R) (2011).
[12] B. Monserrat, N. D. Drummond, and R. J. Needs, Anharmonic vibrational properties in periodic systems: Energy, electron-phonon coupling, and stress, Phys. Rev. B **87**, 144302 (2013).
[13] I. Errea, M. Calandra, and F. Mauri, Anharmonic free energies and phonon dispersions from the stochastic self-consistent harmonic approximation: Application to platinum and palladium hydrides, Phys. Rev. B **89**, 064302 (2014).
[14] T. Tadano and S. Tsuneyuki, Self-consistent phonon calculations of lattice dynamical properties in cubic $SrTiO_3$ with first-principles anharmonic force constants, Phys. Rev. B **92**, 054301 (2015).
[15] S. E. Brown and V. A. Mandelshtam, Self-consistent phonons: An accurate and practical method to account for anharmonic effects in equilibrium properties of general classical or quantum many-body systems, Chem. Phys. **481**, 69 (2016).
[16] V. Kapil, E. A. Engel, M. Rossi, and M. Ceriotti, Assessment of approximate methods for anharmonic free energies, J. Chem. Theory Comput. **15**, 5845 (2019).
[17] R. W. Godby, M. Schlüter, and L. J. Sham, Accurate Exchange-Correlation Potential for Silicon and Its Discontinuity on Addition of an Electron, Phys. Rev. Lett. **56**, 2415 (1986).
[18] R. W. Godby, M. Schlüter, and L. J. Sham, Self-energy operators and exchange-correlation potentials in semiconductors, Phys. Rev. B **37**, 10159 (1988).

[19] R. J. Needs, M. D. Towler, N. D. Drummond, and P. López Ríos, Continuum variational and diffusion quantum Monte Carlo calculations, J. Phys.: Condens. Matter **22**, 023201 (2010).

[20] M. S. Hybertsen and S. G. Louie, Electron correlation in semiconductors and insulators: Band gaps and quasiparticle energies, Phys. Rev. B **34**, 5390 (1986).

[21] C. Gehrmann and D. A. Egger, Dynamic shortening of disorder potentials in anharmonic halide perovskites, Nat. Commun. **10**, 3141 (2019).

[22] M. Sendner, P. K. Nayak, D. A. Egger, S. Beck, C. Müller, B. Epding, W. Kowalsky, L. Kronik, H. J. Snaith, A. Pucci, and R. Lovrinčić, Optical phonons in methylammonium lead halide perovskites and implications for charge transport, Mater. Horiz. **3**, 613 (2016).

[23] A. M. Alvertis, R. Pandya, L. A. Muscarella, N. Sawhney, M. Nguyen, B. Ehrler, A. Rao, R. H. Friend, A. W. Chin, and B. Monserrat, Impact of exciton delocalization on exciton-vibration interactions in organic semiconductors, Phys. Rev. B **102**, 081122(R) (2020).

[24] See Supplemental Material at http://link.aps.org/supplemental/10.1103/PhysRevB.105.L180301 for computational details, an extensive discussion of methods for band-gap calculations, and a (mode-resolved) picture of anharmonicity in acene crystals, which includes Refs. [45–67].

[25] C. E. Patrick and F. Giustino, Unified theory of electronphonon renormalization and phonon-assisted optical absorption, J. Phys.: Condens. Matter **26**, 365503 (2014).

[26] G. Kresse, J. Furthmüller, and J. Hafner, Ab initio force constant approach to phonon dispersion relations of diamond and graphite, Europhys. Lett. **32**, 729 (1995).

[27] K. Parlinski, Z. Q. Li, and Y. Kawazoe, First-Principles Determination of the Soft Mode in Cubic ZrO_2, Phys. Rev. Lett. **78**, 4063 (1997).

[28] A. Singraber, N2P2, https://github.com/CompPhysVienna/n2p2.

[29] J. Behler and M. Parrinello, Generalized Neural-Network Representation of High-Dimensional Potential-Energy Surfaces, Phys. Rev. Lett. **98**, 146401 (2007).

[30] E. A. Engel, V. Kapil, and M. Ceriotti, Importance of nuclear quantum effects for nmr crystallography, J. Phys. Chem. Lett. **12**, 7701 (2021).

[31] V. Kapil and E. A. Engel, A complete description of thermodynamic stabilities of molecular crystals, Proc. Natl. Acad. Sci. USA **119**, e2111769119 (2022).

[32] A. Grisafi and M. Ceriotti, Incorporating long-range physics in atomic-scale machine learning, J. Chem. Phys. **151**, 204105 (2019).

[33] S. N. Pozdnyakov, M. J. Willatt, A. P. Bartók, C. Ortner, G. Csányi, and M. Ceriotti, Incompleteness of Atomic Structure Representations, Phys. Rev. Lett. **125**, 166001 (2020).

[34] F. Brown-Altvater, G. Antonius, T. Rangel, M. Giantomassi, C. Draxl, X. Gonze, S. G. Louie, and J. B. Neaton, Band gap renormalization, carrier mobilities, and the electron-phonon self-energy in crystalline naphthalene, Phys. Rev. B **101**, 165102 (2020).

[35] S. Baroni, S. De Gironcoli, A. Dal Corso, and P. Giannozzi, Phonons and related crystal properties from density-functional perturbation theory, Rev. Mod. Phys. **73**, 515 (2001).

[36] C. Verdi and F. Giustino, Fröhlich Electron-Phonon Vertex from First Principles, Phys. Rev. Lett. **115**, 176401 (2015).

[37] S. Poncé, Y. Gillet, J. Laflamme Janssen, A. Marini, M. Verstraete, and X. Gonze, Temperature dependence of the electronic structure of semiconductors and insulators, J. Chem. Phys. **143**, 102813 (2015).

[38] A. Miglio, V. Brousseau-Couture, E. Godbout, G. Antonius, Y. H. Chan, S. G. Louie, M. Côté, M. Giantomassi, and X. Gonze, Predominance of non-adiabatic effects in zero-point renormalization of the electronic band gap, npj Comput. Mater. **6**, 167 (2020).

[39] Y. N. Wu, W. A. Saidi, J. K. Wuenschell, T. Tadano, P. Ohodnicki, B. Chorpening, and Y. Duan, Anharmonicity explains temperature renormalization effects of the band gap in $SrTiO_3$, J. Phys. Chem. Lett. **11**, 2518 (2020).

[40] A. Troisi, G. Orlandi, and J. E. Anthony, Electronic interactions and thermal disorder in molecular crystals containing cofacial pentacene units, Chem. Mater. **17**, 5024 (2005).

[41] G. Schweicher, G. D'Avino, M. T. Ruggiero, D. J. Harkin, K. Broch, D. Venkateshvaran, G. Liu, A. Richard, C. Ruzié, J. Armstrong, A. R. Kennedy, K. Shankland, K. Takimiya, Y. H. Geerts, J. A. Zeitler, S. Fratini, and H. Sirringhaus, Chasing the "killer" phonon mode for the rational design of low-disorder, high-mobility molecular semiconductors, Adv. Mater. **31**, 1902407 (2019).

[42] H. Seiler, M. Krynski, D. Zahn, S. Hammer, Y. W. Windsor, T. Vasileiadis, J. Pflaum, R. Ernstorfer, M. Rossi, and H. Schwoerer, Nuclear dynamics of singlet exciton fission: A direct observation in pentacene single crystals, Sci. Adv. **7**, eabg0869 (2021).

[43] J. S. Bechtel, J. C. Thomas, and A. Van Der Ven, Finite-temperature simulation of anharmonicity and octahedral tilting transitions in halide perovskites, Phys. Rev. Mater. **3**, 113605 (2019).

[44] http://www.hpc.cam.ac.uk.

[45] J. M. Robertson, V. C. Sinclair, and J. Trotter, The crystal and molecular structure of tetracene, Acta Crystallogr. **14**, 697 (1961).

[46] M. J. Willatt, F. Musil, and M. Ceriotti, Feature optimization for atomistic machine learning yields a data-driven construction of the periodic table of the elements, Phys. Chem. Chem. Phys. **20**, 29661 (2018).

[47] V. Kapil, M. Rossi, O. Marsalek, R. Petraglia, Y. Litman, T. Spura, B. Cheng, A. Cuzzocrea, R. H. Meißner, D. M. Wilkins, B. A. Helfrecht, P. Juda, S. P. Bienvenue, W. Fang, J. Kessler, I. Poltavsky, S. Vandenbrande, J. Wieme, and M. Ceriotti, i-PI 2.0: A universal force engine for advanced molecular simulations, Comput. Phys. Commun. **236**, 214 (2019).

[48] Y. Eldar, M. Lindenbaum, M. Porat, and Y. Y. Zeevi, The farthest point strategy for progressive image sampling, IEEE Trans. Image Process. **6**, 1305 (1997).

[49] V. Kapil, J. Behler, and M. Ceriotti, High order path integrals made easy, J. Chem. Phys. **145**, 234103 (2016).

[50] G. Imbalzano, A. Anelli, D. Giofré, S. Klees, J. Behler, and M. Ceriotti, Automatic selection of atomic fingerprints and reference configurations for machine-learning potentials, J. Chem. Phys. **148**, 241730 (2018).

[51] B. Hourahine, B. Aradi, V. Blum, F. Bonafé, A. Buccheri, C. Camacho, C. Cevallos, M. Y. Deshaye, T. Dumitric, A. Dominguez, S. Ehlert, M. Elstner, T. van der Heide, J. Hermann, S. Irle, J. J. Kranz, C. Köhler, T. Kowalczyk, T. Kuba, I. S. Lee *et al.*, DFTB+, a software package for efficient approximate

density functional theory based atomistic simulations, J. Chem. Phys. **152**, 124101 (2020).

[52] F. Musil, M. J. Willatt, M. A. Langovoy, and M. Ceriotti, Fast and accurate uncertainty estimation in chemical machine learning, J. Chem. Theory Comput. **15**, 906 (2019).

[53] M. Gaus, A. Goez, and M. Elstner, Parametrization and benchmark of DFTB3 for organic molecules, J. Chem. Theory Comput. **9**, 338 (2013).

[54] S. C. Capelli, A. Albinati, S. A. Mason, and B. T. M. Willis, Molecular motion in crystalline naphthalene: Analysis of multi-temperature x-ray and neutron diffraction data, J. Phys. Chem. A **110**, 11695 (2006).

[55] P. Giannozzi, S. Baroni, N. Bonini, M. Calandra, R. Car, C. Cavazzoni, D. Ceresoli, G. L. Chiarotti, M. Cococcioni, I. Dabo, A. Dal Corso, S. Fabris, G. Fratesi, S. de Gironcoli, R. Gebauer, U. Gerstmann, C. Gougoussis, A. Kokalj, M. Lazzeri, L. Martin-Samos *et al.*, QUANTUM ESPRESSO: A modular and open-source software project for quantum simulations of materials, J. Phys.: Condens. Matter **21**, 395502 (2009).

[56] M. A. Morales, J. M. McMahon, C. Pierleoni, and D. M. Ceperley, Towards a predictive first-principles description of solid molecular hydrogen with density functional theory, Phys. Rev. B **87**, 184107 (2013).

[57] A. P. Bartók, R. Kondor, and G. Csányi, On representing chemical environments, Phys. Rev. B **87**, 184115 (2013).

[58] A. Tkatchenko and M. Scheffler, Accurate Molecular Van Der Waals Interactions from Ground-State Electron Density and Free-Atom Reference Data, Phys. Rev. Lett. **102**, 073005 (2009).

[59] M. Rossi, P. Gasparotto, and M. Ceriotti, Anharmonic and Quantum Fluctuations in Molecular Crystals: A First-Principles Study of the Stability of Paracetamol, Phys. Rev. Lett. **117**, 115702 (2016).

[60] J. P. Perdew, K. Burke, and M. Ernzerhof, Generalized Gradient Approximation Made Simple, Phys. Rev. Lett. **77**, 3865 (1996).

[61] M. Ceriotti, M. Parrinello, T. E. Markland, and D. E. Manolopoulos, Efficient stochastic thermostatting of path integral molecular dynamics, J. Chem. Phys. **133**, 124104 (2010).

[62] M. Gaus, X. Lu, M. Elstner, and Q. Cui, Parameterization of DFTB3/3OB for sulfur and phosphorus for chemical and biological applications, J. Chem. Theory Comput. **10**, 1518 (2014).

[63] Y. Tajima, T. Matsuo, and H. Suga, Phase transition in KOH-doped hexagonal ice, Nature (London) **299**, 810 (1982).

[64] H. J. Monkhorst and J. D. Pack, Special points for Brillouin-zone integrations, Phys. Rev. B **13**, 5188 (1976).

[65] S. Haas, B. Batlogg, C. Besnard, M. Schiltz, C. Kloc, and T. Siegrist, Large uniaxial negative thermal expansion in pentacene due to steric hindrance, Phys. Rev. B **76**, 205203 (2007).

[66] G. Imbalzano and M. Ceriotti, Modeling the Ga/As binary system across temperatures and compositions from first principles, Phys. Rev. Materials **5**, 063804 (2021).

[67] B. Cheng, E. A. Engel, J. Behler, C. Dellago, and M. Ceriotti, Ab initio thermodynamics of liquid and solid water, Proc. Natl. Acad. Sci. USA **116**, 1110 (2019).

Correction: The values along the x axis of the previously published Fig. 2(c) were inconsistent with units reflected elsewhere in the paper. Figure 2 has been replaced to resolve the discrepancy. Corresponding changes to the Supplemental Material have also been made.